

Aftershock Fragility Curves for Damaged Non-Ductile Reinforced Concrete Buildings

J.S. Jeon, R. DesRoches & I. Brilakis

Georgia Institute of Technology, Atlanta, USA

L.N. Lowes

University of Washington, Seattle, USA



SUMMARY:

The objective of this paper is to evaluate the seismic cumulative damage potential of non-ductile reinforced concrete (RC) buildings, including the effect of multiple earthquakes on their performance and increased vulnerability. The motivation stems from the fact that buildings that survived a mainshock may sustain additional damage or collapse when subjected to aftershocks. The analytical model of a non-ductile RC frame in OpenSees was implemented and validated by comparing the analytical and experimental results available in the literature. Fragility curves of damaged buildings using coupled pushover and nonlinear time history analysis were developed and characterized in terms of an aftershock intensity measure and an initial damage state using a suite of ground motions. Furthermore, to quantitatively estimate the post-earthquake vulnerability assessment for damaged buildings, the fragility curves were compared with different initial damage states, the extent of which governs the shapes of those curves.

Keywords: non-ductile reinforced concrete, multiple earthquakes, damaged building, aftershock fragility curve

1. INTRODUCTION

Although the knowledge and technology of seismic analysis and seismic risk assessment tools have rapidly advanced in the past several decades, current seismic design codes neglect the effect of multiple earthquakes on structures. However, in light of recent strong seismic events (the 1994 Northridge earthquake, USA, Hauksson and Jones 1995; the 1999 Kocaeli earthquake, Turkey, USGS 2000; the 2010 Darfield and 2011 Christchurch earthquakes, New Zealand, Smyrou et al. 2011), all of which were followed by many aftershocks, structures are more vulnerable to severe damage and collapse. Such increased vulnerability associated with a mainshock and its aftershocks significantly threatens the safety of occupants in these structures. Moreover, a structure damaged by a mainshock may be incapable of resisting the excitation of a strong aftershock, not only increasing the risk of major damage or building collapse but also causing additional loss of life and property.

In spite of increased interest in the effect of multiple earthquakes (mainshock-aftershock sequence), very few studies have investigated the seismic performance of structures under multiple earthquakes. Aschheim and Black (1999) proposed the hysteretic pinching model of single degree of freedom (SDOF) oscillators to account for the effect of prior earthquakes. However, this study is limited because the effect of prior earthquakes was represented as only stiffness degradations. Amadio et al. (2003) investigated the nonlinear response of SDOF systems, but they accounted for only one natural and two artificial ground motions. Haziorgiou and Liolios (2010) conducted an extensive parametric study on the inelastic response of eight low- and mid-rise reinforced concrete (RC) frames subjected to 45 repeated ground motions that consisted of five real and 40 artificial seismic sequences. They concluded that multiple earthquakes require increased displacement (ductility) demands compared to single earthquakes. Ruiz-García and Negrete-Manriquez (2011) evaluated the effect of as-recorded aftershocks (far-field and near-fault) on peak and residual drift demands in steel frame buildings. They found that the frequency content of mainshock and aftershock ground motions, such as the predominant period of ground motion and the bandwidth, is weakly correlated through statistical observation.

Bazzurro et al. (2004) proposed parameterized pushover load analyses to develop the aftershock fragility curves of steel frames. They converted nonlinear pushover curves into incremental dynamic analysis (IDA) curves using the SPO2IDA tool (Vamvatsikos and Cornell 2006) and then developed aftershock fragility curves. However, their approach overestimated the residual deformation capacity obtained from backward pushover in comparison with nonlinear time history analysis, and it did not account for the effect of cyclical degradation (stiffness and strength degradation), which increases seismic demand. Ryu et al. (2012) generated mainshock ground motions with specific damage states for SDOF systems through IDA, and they performed back-to-back dynamic analyses for mainshock-aftershock sequences to develop collapse fragility curves. However, the idealization of multi-story structures with SDOF representations will not yield accurate results. Furthermore, this approximation suffers from the inability to capture damage localized in different parts of a structure, primarily the joints.

The purpose of this paper is to evaluate the seismic cumulative damage potential of non-ductile RC buildings by accounting for the effect of multiple earthquakes on their increased vulnerability. Accurate estimations of cumulative damage under multiple earthquakes necessitate the development of an analytical model of these buildings. In this study, an analytical model was built in OpenSees (McKenna et al. 2010). This model was validated by comparing analytical results with the experimental results available in the literature. To simulate the effect of mainshocks on these buildings, this paper proposed an efficient, effective, and reliable analysis technique by replacing ground motions with cyclic pushover analyses. The coupled pushover and nonlinear time history analyses enable us to develop aftershock fragility curves with different initial damage states caused by mainshocks. A comparison of these curves can assess the post-earthquake vulnerability of damaged buildings.

2. AFTERSHOCK FRAGILITY METHODOLOGY

This section assesses the increased vulnerability of non-ductile RC buildings subjected to multiple earthquakes by developing aftershock fragility curves of these structures. Mainshock fragility is a conditional probability statement of damage that depends on a mainshock intensity measure while aftershock fragility is a conditional probability that determines the likelihood that a damaged structure will meet or exceed a specified level of damage, given an aftershock intensity measure (IM_{as}) and an initial damage state (IDS) associated with the mainshock. The aftershock fragility reflects the increased vulnerability of structures as a result of the mainshock. The mainshock fragility curves are based on nonlinear time history analyses for the estimation of the mainshock seismic demand while the aftershock fragility curves developed herein are based on coupled pushover (hypothetical mainshock) and nonlinear time history (aftershock) analyses for the evaluation of the aftershock seismic demand. Given lognormal distributions for both structural capacity (C) and seismic demand (D), common fragility curves can be solved in closed form, as given in Eqn. (2.1):

$$P[D > C | IM] = \Phi \left[\frac{\ln(S_d / S_c)}{\sqrt{\beta_{d|IM}^2 + \beta_c^2 + \beta_m^2}} \right] \quad (2.1)$$

where IM is the intensity measure of ground motions; S_d and $\beta_{d|IM}$ are the median value and dispersion, respectively, of the demand as a function of I ; S_c and β_c are the median value and dispersion, respectively, of the capacity; β_m is the modeling uncertainty ($\beta_m=0.2$, Celik and Ellingwood 2010); and $\Phi[\cdot]$ is the standard normal distribution function. With the addition of the mainshock initial damage state, the aftershock fragility curves can be written as follows:

$$P[D_{as} > C | IM_{as}, IDS] = \Phi \left[\frac{\ln(S_d / S_c)}{\sqrt{\beta_{d|IM_{as}}^2 + \beta_c^2 + \beta_m^2}} \right] \quad (2.2)$$

where D_{as} is the aftershock demand for damaged structures; IDS is the initial damage state induced by the mainshock; and $\beta_{d|IM_{as}}$ is the dispersion of the aftershock demand for mainshock-damaged structures conditioned on the IM_{as} .

The basic procedure for generating the aftershock fragility curves in this study is summarized by the following steps:

- Generate N statistical samples of the subject frame. These samples can be generated by sampling on different, significant modeling parameters. Thus, N nominally identical but statistically significant frame samples are generated through Latin hypercube sampling (LHS).
- Assemble a suite of N ground motions that are applicable to the area of interest.
- Characterize hypothetical mainshocks (cyclic pushover loadings) that can simulate the effect of a mainshock on structures (initial damage state due to a mainshock).
- Perform a full nonlinear time history analysis for each aftershock ground motion-frame pair. Peak responses, engineering demand parameters (EDP) such as interstory and roof drift ratios, are monitored along with the aftershock intensity measure.
- Generate an aftershock probabilistic seismic demand model (PSDM), a linear regression of the demand-intensity measure pairs in the log-transformed space.
- Develop aftershock fragility curves with different initial damage states using Eqn. 2.2.

3. ANALYTICAL MODELING OF NON-DUCTILE RC BUILDINGS

This section provides a detailed description of a one-third scale model frame along with information about the analytical modeling procedure and presents the validation of the analytical model of this frame.

3.1. Description of the Scale Model Frame

The model frame chosen in this study is a one-third scale three-story, three-bay reinforced concrete frame designed and constructed by Bracci et al. (1995). The prototype building was designed for only gravity loads without seismic provisions in accordance with ACI 318-89 (1989). The model frame represents the interior frame of the prototype building for a shake-table test at the University of Buffalo, New York. The input ground motion was the N21E component of the 1952 Taft earthquake scaled to be 0.2g, with the excitation time of $1/\sqrt{3}$. Figure 11 illustrates the geometry of the model frame used in the experimental work of Bracci et al. (1995). As shown in the figure, this non-ductile RC frame has inadequate column shear capacity due to a lack of confinement and poor reinforcement details, lap splice of column reinforcement in its potential plastic hinge regions, and weak joints due to limited shear capacity associated with little or no joint transverse reinforcement and inadequate anchorage of bottom beam reinforcement. Further details on the material properties and reinforcement details can be found in Bracci et al. (1995).

3.2. Analytical Model of the Scale Model Frame

Figure 2 shows the analytical model of the scale model frame. The analytical model is implemented in the finite element platform OpenSees (McKenna, 2010). The columns and beams are modeled as beamWithHinges elements developed by Scott and Fenves (2006). The beamWithHinges element is composed of three parts: two plastic hinge zones (fiber sections) at the ends of the element and linear elastic region (effective stiffness) in the middle of the element. The plastic hinge length of a member can be estimated using equation proposed by Paulay and Priestley (1992);

$$l_p = 0.08l + 0.022d_b f_y \quad (\text{MPa}) \quad (3.1)$$

where l is the length of the member; and f_y and d_b are the yield strength and diameter, respectively, of

the longitudinal reinforcing bars. The fiber-defined cross-sections facilitate the specification of different properties for cover and core concrete that can account for the effects of confinement and ductility. The model of Mander et al. (1988) accounts for the enhanced compressive strength and ductility of core concrete associated with the confinement factor. The longitudinal reinforcement of elements was employed using Steel02 based on the Giuffr -Menegotto-Pinto model. The effective width of the slab can be calculated using the equations proposed by Paulay and Priestley (1992). In addition, the effective stiffness of the elastic material can be obtained following the recommendation of FEMA 356 (2000).

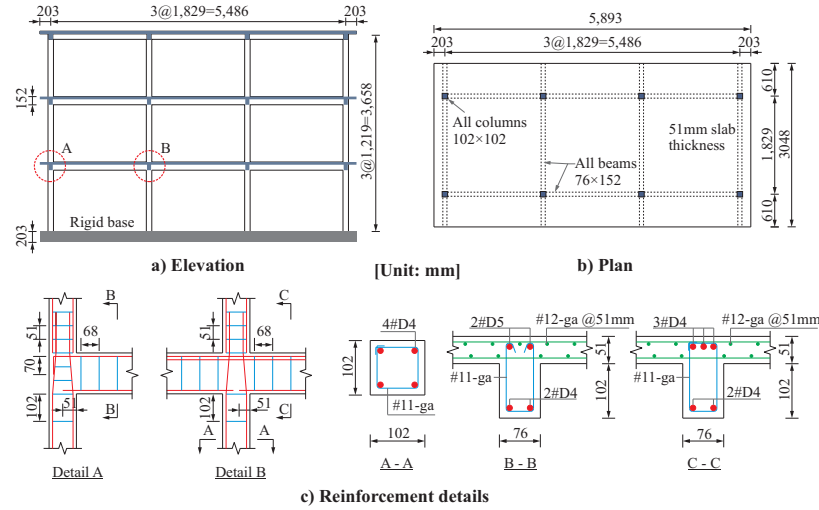


Figure 1. Geometry and reinforcement details of the scale model frame (Bracci et al. 1995)

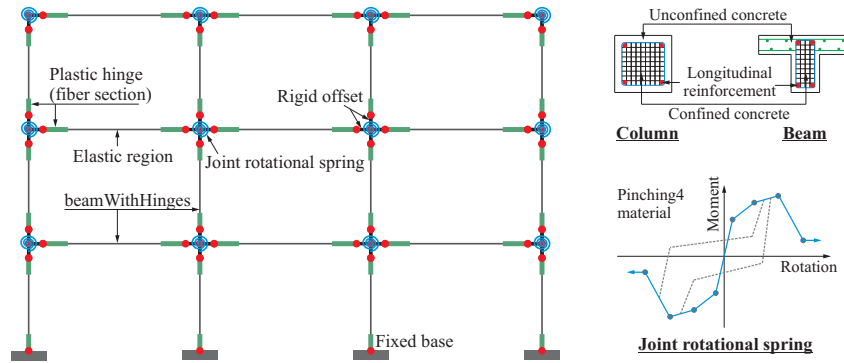


Figure 2. Analytical model of the scale model frame

The joint panel can be represented as four rigid offsets with one zero-length rotational spring, as shown in Figure 2. The joint rotational spring is modeled using Pinching4 material (available in OpenSees) developed by Lowes and Altoontash (2003), which provides a detailed description of this material. The envelope curve of the joint moment-rotational spring can be estimated following the approach of Celik and Ellingwood (2008) but with a modification to the effect of bond slip in or adjacent to a joint. This bond slip can be addressed by adopting the bilinear material with the reduction of steel strength for bottom discontinuous beam reinforcements. The strength of this material can be modified by

$$f_s = f_y \times l_b / l_d \quad (3.2)$$

where f_s is the maximum steel stress, f_y the steel yield stress, l_b the provided embedment length, and l_d the development length required by ACI 318-08 (2008). The joint cracking moment as a result of

shear stress carried by the concrete can be calculated using the equation recommended by ACI-ASCE Committee 352 (1976). The equation for the joint rotational moment can be derived from the geometry of the structure and the equilibrium of forces, as indicated in Figure 3. In addition, four yield and ultimate end moments of members adjacent to the joint panel can be obtained through a moment-curvature analysis, and the yield and ultimate moment of the joint can be determined by taking the lesser of these joint moments induced by beam and column shears. The joint residual moment is assumed to be 80% of the joint ultimate moment. Furthermore, joint shear strains can be indirectly estimated by using the drift contributions and equations in Aycardi et al. (1994), who conducted cyclic pushover tests for interior and exterior subassemblages of the scale model frame. The validation of analytical model of these subassemblages can be found in Jeon et al. (2012).

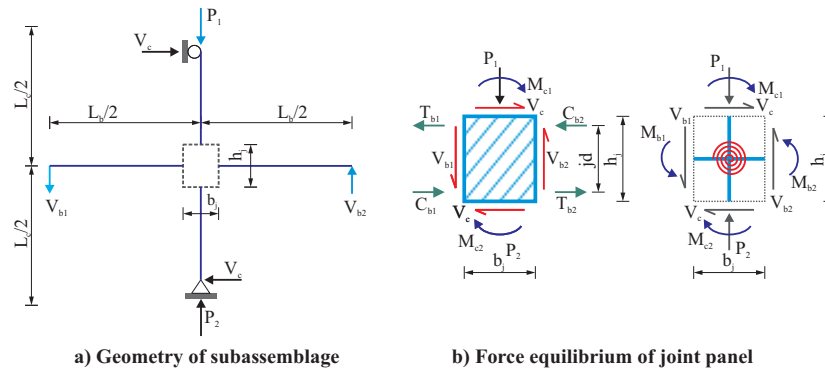


Figure 3. Structural geometry and force equilibrium (Celik and Ellingwood 2008)

Lumped mass at every connection was employed, and the 2% Rayleigh damping in the first two modes was used for dynamic analysis. An eigenvalue analysis of the scale model frame revealed a fundamental period of approximately 0.67 seconds. As mentioned before, the input ground motion was the N21 component of the 1952 Taft earthquake. Figure 4 indicates that the peak ground acceleration (PGA) of the excitation is 0.2g.

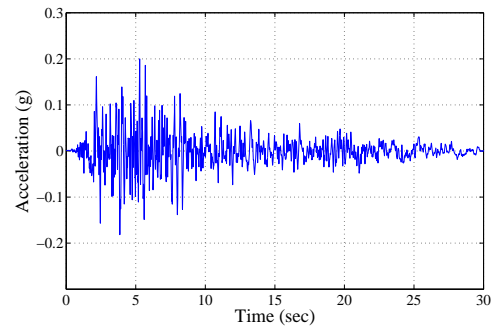


Figure 4. Input motion (Bracci et al. 1995)

Figures 5a) and 5b) illustrate the comparisons of roof displacement and base shear force time history responses of the Bracci et al. (1995) experiment with those of the time history analysis. The displacement time history matches the experimental results well. The amplitude decayed after a peak value of the displacement response near 5 seconds, as shown in Figure 5a). However, the amplitude increased between 18 and 23 seconds. It can be indicated that the strength and stiffness degradation during unloading and reloading occurred during this time period. The analytical model accurately captured degradation in the strength and stiffness of the experimental structure. Although the analytical results slightly underestimate the base shear forces, as presented in Figure 5b), the overall shear force response accurately predicted the actual response.

4. AFTERSHOCK FRAGILITY CURVES OF NON-DUCTILE RC BUILDINGS

This section assesses the increased vulnerability of non-ductile RC buildings subjected to multiple earthquakes by developing aftershock fragility curves for these structures. This study involves the probabilistic analytical modeling technique for these structures, the selection of a suite of ground motions, the characterization of hypothetical mainshocks (cyclic pushover), and the development of an aftershock probabilistic seismic demand model (PSDM) and aftershock fragility curves with different initial damage states induced by mainshocks.

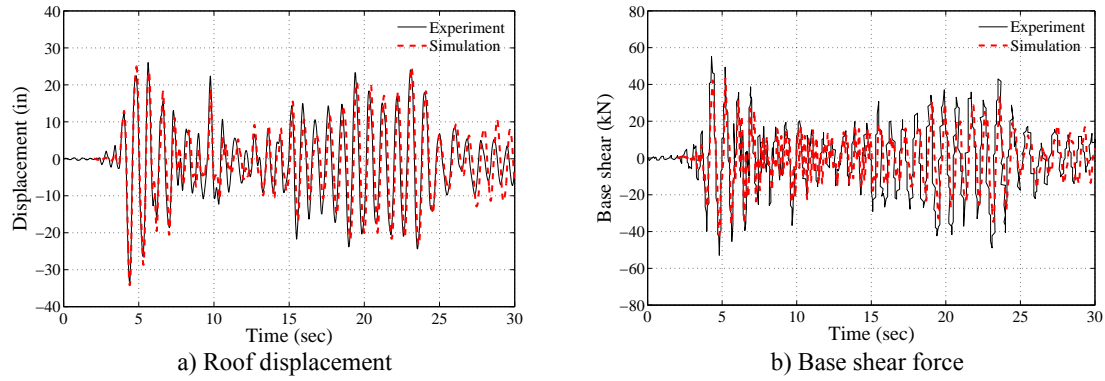


Figure 5. Comparison between time history responses of the experiment (Bracci et al. 1995) and those of the analysis

4.1. Probabilistic Structural Models

The analytical models of non-ductile RC frames, including both geometrical and material nonlinearities, are implemented in the finite element program OpenSees. Figure 6 shows a prototype of the scale model frame designed under the factored load combination of 1.4D (dead load) + 1.7L (live load) (Bracci et al. 1995). The total slab dead and live loads are 5.27 kips and 2.4 kips, respectively. The lumped masses are employed at each beam-column connection based on the gravity load combination of 1.05D + 0.25L. As mentioned in the previous section, the columns and beams are modeled as the beamWithHinges element. The joint rotational moments can be obtained from the modified model of Celik and Ellingwood (2008). Moreover, the joint shear strains (rotations) can be estimated following the unified equations proposed by Kim and LaFave (2009), who examined 341 experimental data for interior and exterior subassemblages with and without joint transverse reinforcement. These equations depend on the yield strength of longitudinal reinforcement, the compressive strength of concrete, and the type of connection (interior, exterior, and knee joints). Uncertainties in the modeling parameters such as the concrete compressive strength, the steel yield strength, and the damping ratio are incorporated in the frame models using the LHS technique, one of the variance reduction techniques of Monte Carlo simulation. The probability distributions of these modeling parameters were investigated by Healy et al. (1980), as presented in Table 4.1.

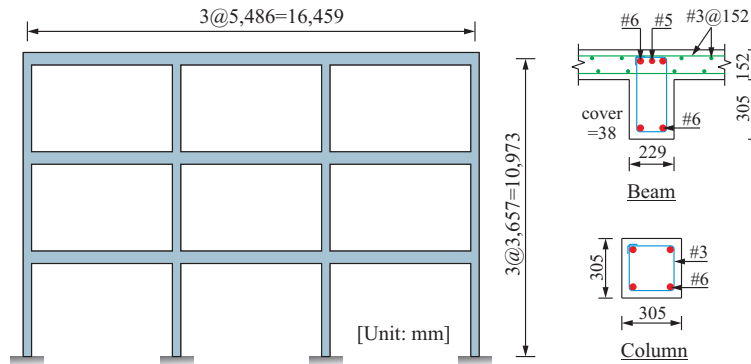


Figure 6. Typical three-story, three-bay non-ductile RC frame (Bracci et al. 1995)

Table 4.1. Structural Modeling Uncertainties (Healy et al. 1980)

Parameter	Probability distribution	Mean	Coefficient of variation
Concrete compressive strength	Normal (N)	34.5 MPa	0.18
Steel yield strength	Lognormal (LN)	345 MPa	0.11
Damping ratio	Lognormal (LN)	4.26%	0.76

4.2. Selection of Ground Motions

To generate the fragility curves of the RC frames, a suite of ground motions (Baker et al. (2011)) were chosen in this study. The suite of ground motions consists of four sets: Set 1A (broad-band, magnitude=7, distance to rupture=10km, soil site), Set 1B (broad-band, magnitude=6, distance to rupture=25km, soil site), Set 2 (broad-band, magnitude=7, distance to rupture=10km, rock site), and Set 3 (near-fault). Each ground motion set consists of 40 two-component ground motions (a total of 160 pairs). To reduce the time-consumption of the runs, 20 ground motions for each set that represented the original suite were re-assembled. To obtain the suite of 80 ground motions used for analyzing the structural models, the distribution of PGAs for each set is assumed to be lognormal, as exhibited in Figure 7, and the LHS technique is exploited to extract the random samples of the PGAs. Finally, ground motions with PGA values chosen are close to those sampled from the distribution. In the figure, λ and ζ are the parameters of the lognormal distribution, which means that these parameters are, respectively, the mean and standard deviation of $\ln(PGA)$.

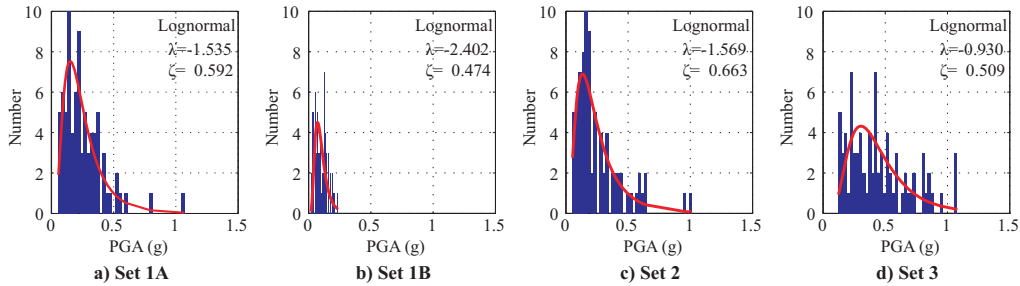


Figure 7. Probability density function (PDF) of the PGAs

4.3. Coupled Pushover (Hypothetical Mainshock) and Nonlinear Time History Analysis

To simulate the effect of mainshock ground motions on the structures, cyclic pushover loading was applied to the structures instead of earthquake loadings. Bazzurro et al. (2004) used successive nonlinear static pushover analyses to capture the post-elastic behavior of a steel moment-resisting frame (SMRF). After loading or reloading to the specified limit states, the reloading stops when the base shear is zero. At this point, they defined the residual roof deformation (or drift) as the residual capacity of this frame. Then using the SPO2IDA tool (Vamvatsikos and Cornell 2006), they generated the collapse fragility curves for this frame by converting the capacity curve into IDA curve. However, their approach did not account for degradation in stiffness and strength associated with the effect of loading cycles, and it overestimated the residual roof drift compared to the drift of the nonlinear time history analysis. To overcome the drawbacks of their approach, the modified the pushover load pattern was applied to undamaged structures, and aftershock earthquakes subsequently imposed on damaged structures, as presented in Figure 8. In the figure, the loading gradually increases to the specific maximum roof drift associated with initial damage states and decreases symmetrically until the base shear is zero (residual roof drift). The initial damage states chosen in this study are six different damage states corresponding to maximum roof drifts: no initial damage (IDS0), 0.5% (IDS1), 1.0% (IDS2), 1.5% (IDS3), 2.0% (IDS4), and 2.5% (IDS5). (Using the experimental data of shear-critical columns available in the literature, the maximum drift ratio will be identified later.) A cyclic pushover analysis of the hypothetical mainshock response was performed and then a nonlinear time history analysis of the aftershock response was conducted. In addition, both positive and negative factors of aftershock ground motions were applied to damaged structures because aftershock peak responses depend on the polarity of aftershock ground motions (Ryu et al. 2011).

4.4. Aftershock Probabilistic Seismic Demand Models

For each aftershock motion-frame pair, a nonlinear time history analysis was performed, and the roof and interstory drift responses were monitored. Given the lognormal distribution of seismic demand, a

linear regression of the demand-intensity measure pairs in the log-transformed space, the so-called probabilistic seismic demand model (PSDM), determines the median, the dispersion (σ), the slope, and the coefficient of determination (R^2). In this work, this PSDM relates the IM (i.e., the spectral acceleration at the fundamental period of a damaged structure (S_{a-T1})) to the EDP (i.e., the maximum interstory drift ratio (θ_{max})). Figure 9a shows the PSDM for 80 sequences of pushover loadings with a moderate initial damage state (IDS2) followed by aftershock ground motions. Figure 9b illustrates the aftershock fragility curves with different initial damage states. This figure indicates that the more damage a structure initially sustains, the higher the seismic demand in subsequent earthquakes.

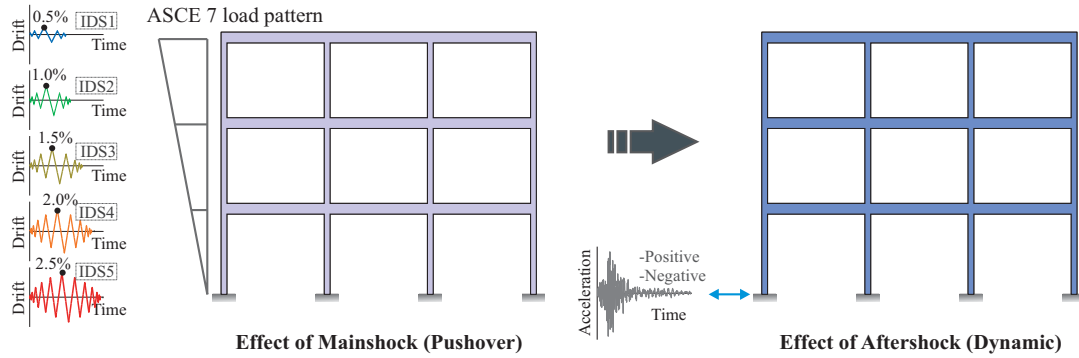


Figure 8. Cyclic pushover load pattern

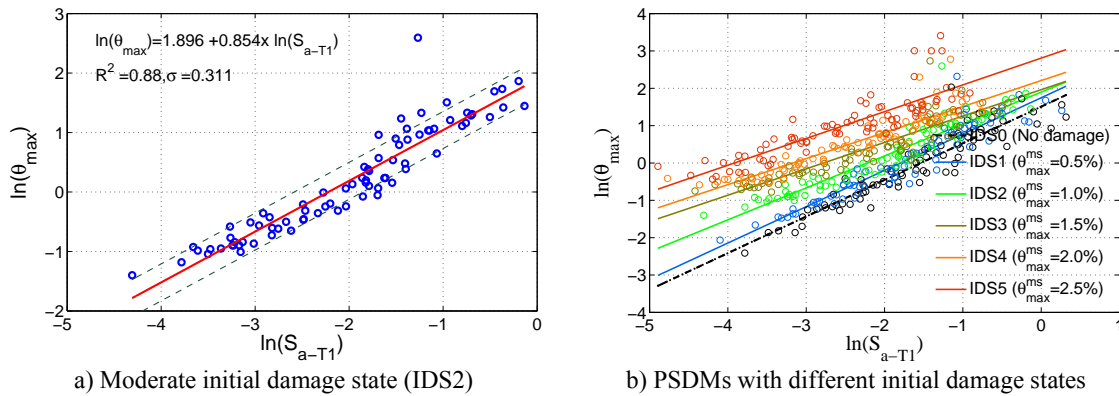


Figure 9. Aftershock PSDMs

4.5. Aftershock Fragility Curves

The capacity limit state for maximum interstory drift (%) is assumed to lognormal distributed. Following HAZUS-MH (FEMA 2003), the median values (S_c) for four damage states (slight=0.5, moderate=0.8, extensive=2.0, and complete=5.0) were employed, and the capacity dispersion (β_c) for all damage states is assumed to be 0.25. Using Eqn. 2.2, aftershock fragility curves were generated with the aftershock PSDMs and the capacity limit states. Figure 11 illustrates the resulting aftershock fragility curves with different initial damage states for the analyzed non-ductile RC frames. As presented in the figures, an aftershock fragility curve with an initially severe damage state takes on a steeper slope. For example, when a frame is subject to an aftershock with S_{a-T1} of 0.4g, comparison of IDS0 (undamaged) and IDS1 (damaged) indicates that an aftershock would have a 50% increased probability of failure for extensive damage state, as shown in Figure 11(b). Therefore, given the specific intensity measure, this aftershock fragility curve conditioned on an initially severe damage state has a higher failure probability, resulting in increased vulnerability of structures subjected to multiple earthquakes.

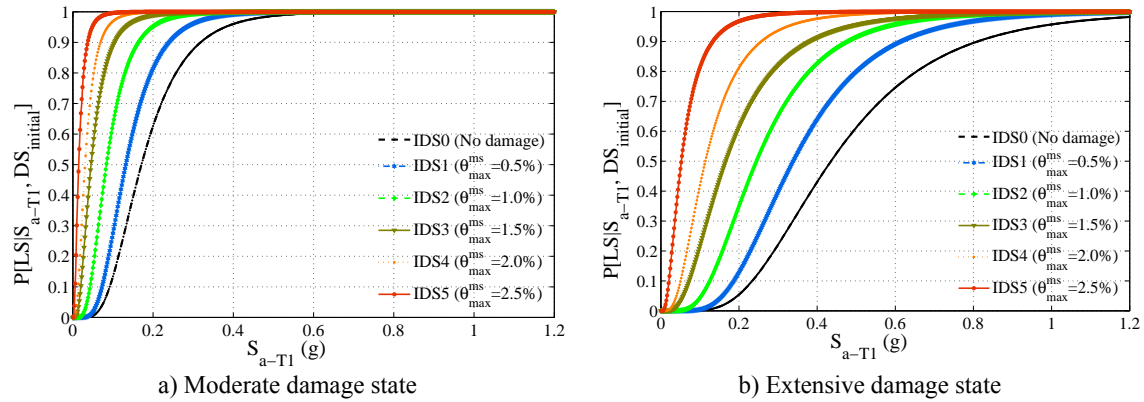


Figure 11. Aftershock fragility curves for PSDMs with moderate and complete damage states

5. SUMMARY AND CONCLUSION

The paper proposes an analytical procedure for the generation of aftershock fragility curves for a non-ductile RC building representative of a three-story, three-bay RC building designed for a gravity-load combination. To assess its increased vulnerability, a reliable analytical model that was created in OpenSees was developed and was validated by comparing the analytical results of the simulation with experimental results of a shake-table test for a scale model frame. The analytical predictions show good agreement with the experimental results. In addition, probabilistic analytical models sampled by LHS were generated and were subjected to coupled pushover and nonlinear time history analyses. Aftershock PSDMs were developed in terms of a spectral acceleration at the fundamental period of a damaged structure and maximum interstory drift. The PSDMs indicated that the more damage a structure initially sustains, the higher the seismic demand in subsequent earthquakes. Moreover, applying limit states and the aftershock PSDMs, aftershock fragility curves with different initial damage states were generated and compared, providing evidence that the more damage a structure initially sustains, the higher the seismic demand when the structure is subjected to same aftershock ground motions. For example, when a frame is subject to an aftershock with S_{a-T1} of 0.4g, comparison of IDS0 (undamaged) and IDS1 (damaged) indicates that an aftershock would have a 50% increased probability of failure for extensive damage state. Since the proposed approach provides simpler, more reliable, and more visible results, it provides a more quantitative evaluation of the cumulative damage potential of structures subjected to multiple earthquakes.

ACKNOWLEDGEMENTS

This research was supported by the National Science Foundation under NSF Grant # 1000700. However, the views expressed are solely those of the authors and may not represent the position of the NSF. The authors also thank Professor Joseph M. Bracci of Texas A&M University, who shared the experimental results for the shake-table test.

REFERENCES

- ACI-ASCE Committee 352 (1976). Recommendations for design of beam-column joints in monolithic reinforced concrete structures. *ACI Journal* **73**:7,375-393.
- ACI Committee 318 (1989). Building Code Requirements for Reinforced Concrete (ACI318-89) and Commentary (318R-89), American Concrete Institute, Detroit, M.I.
- ACI Committee 318 (2008). Building Code Requirements for Reinforced Concrete (ACI318-08) and Commentary, American Concrete Institute, Farmington Hills, M.I.
- Amadio, C., Fragiaco, M. and Rajgelj, S. (2003). The effects of repeated earthquake ground motions on the non-linear response of SDOF systems, *Earthquake Engineering and Structural Dynamics* **32**:2,291-308.

- Aschheim, M. and Black, E. (1999). Effects of prior earthquake damage on response of simple stiffness-degrading structures, *Earthquake Spectra* **15:1**,1-24.
- Aycardi, L.E., Mander, J.B. and Reinhorn, A.M. (1994). Seismic resistance of reinforced concrete frame structures designed only for gravity loads: Experimental performance of subassemblages. *ACI Structural Journal* **91:5**,552-563.
- Baker, J.W., Shahi, S.K. and Jayaram, N. (2011). New Ground Motion Selection Procedures and Selected Motions for the PEER Transportation Research Program, PEER Report 2011/03, Pacific Earthquake Engineering Research Center, University of California, Berkeley, C.A.
- Bazzurro, P., Cornell, C.A., Menun, C. and Motahari, M. (2004). Guidelines for Seismic Assessment of Damaged Buildings. *Thirteenth World Conference on Earthquake Engineering*, Paper No. 1708, Vancouver, Canada.
- Bracci, J.M., Reinhorn, A.M. and Mander, J.B. (1995). Seismic resistance of reinforced concrete frame structures designed for gravity loads: Performance of structural system. *ACI Structural Journal* **92:5**,597-608.
- Celik, O.C. and Ellingwood, B.R. (2008). Modeling beam-column joints in fragility assessment of gravity load designed reinforced concrete frames. *Journal of Earthquake Engineering* **12:3**,357-381.
- Celik, O.C. and Ellingwood, B.R. (2010). Seismic fragilities for non-ductile reinforced concrete frames –Role of aleatoric and epistemic uncertainties. *Structural Safety* **32:1**,1-12.
- FEMA (2003). HAZUS-MH MR4 Technical Manual, Earthquake Model, Federal Emergency Management Agency, Washington, D.C.
- FEMA 356 (2000). Prestandard and Commentary for the Seismic Rehabilitation of Buildings, FEMA Publication No. 356, prepared by the American Society of Civil Engineers for the Federal Emergency Management Agency, Washington, D.C.
- Hatzigeorgiou, G.D. and Liolios, A.A. (2010). Nonlinear behaviour of RC frames under repeated strong ground motions, *Soil Dynamics and Earthquake Engineering* **30:10**,1010-1025
- Hauksson, E. and Jones, L.M. (1995). The 1994 Northridge earthquake sequence in California: Seismological and tectonic aspects, *Journal of Geophysical Research* **100:B7**,12335-12355.
- Healy, J.J., Wu, S.T. and Murga M. (1980). Structural Building Response Review. NUREG/CR-1423, Vol. 1, US Nuclear Regulatory Commission, Washington, D.C.
- Jeon, J.S., DesRoches, R., Brilakis, I. and Lowes, L.N. (2012). Modeling and Fragility Analysis of Non-Ductile Reinforced Concrete Buildings in Low-to-Moderate Seismic Zones. *Proceedings of the 2012 Structures Congress*,2199-2210.
- Kim, J. and LaFave, J.M. (2009). Joint Shear Behavior of Reinforced Concrete Beam-Column Connections Subjected to Seismic Lateral Loading. Report No. NSEL-020, Department of Civil and Environmental Engineering, University of Illinois at Urbana-Champaign, I.L.
- Lowes, L.N. and Altoontash, A. (2003). Modeling reinforced-concrete-column joints subjected to cyclic loadings. *ASCE Journal of Structural Engineering* **129:12**,1686-1679.
- Mander, J.B., Priestley, M.J.N. and Park, R. (1988). Theoretical stress-strain model for confined concrete. *ASCE Journal of Structural Engineering* **114:8**,1804-1826.
- McKenna, F., Scott, M.H. and Fenves, G.L. (2010). Nonlinear finite-element analysis software architecture using object composition. *ASCE Journal of Computing in Civil Engineering* **24:1**,95-107.
- Ruiz-García, J. and Negrete-Manriquez, J.C. (2011). Evaluation of drift demands in existing steel frames under as-recorded far-field and near-fault mainshock-aftershock seismic sequences, *Engineering Structures* **33:2**,621-634.
- Ryu, H., Luco, N., Uma, S.R. and Liel, A.B. (2011). Developing Fragilities for Mainshock-Damaged Structures Through Incremental Dynamic Analysis. *Proceedings of the Ninth Pacific Conference on Earthquake Engineering*, Paper No. 225, Auckland, New Zealand.
- Paulay, T. and Priestley, M.J.N. (1992). *Seismic Design of Reinforced Concrete and Masonry Buildings*, Wiley & Sons, Inc., N.Y.
- Scott, M.H. and Fenves, G.L. (2006). Plastic hinge integration methods for force-based beam-column elements. *ASCE Journal of Structural Engineering* **132:2**,244-252.
- Smyrou, E., Tasiopoulou, P., Bal, I.E., Gazetas, G. and Vintzileou, E. (2011). Structural and Geotechnical Aspects of the Christchurch (2011) and Darfield (2010) Earthquakes in N.Zealand, *Seventh National Conference on Earthquake Engineering*, Istanbul, Turkey.
- U.S. Geological Survey (2000). Implications for Earthquake Risk Reduction in the United States from the Kocaeli, Turkey, Earthquake of August 17, 1999. U.S. Geological Survey Circular 1182.
- Vamvatsikos, D. and Cornell, C.A. (2006). Direct estimation of the seismic demand and capacity of oscillators with multi-linear static pushovers through IDA. *Earthquake Engineering and Structural Dynamics* **35:9**,1097-1117.